Transient photoexcited state of the small-gap quasi-two-dimensional Mott-Hubbard insulator Sn/Si(111)-($\sqrt{3} \times \sqrt{3}$)-R30°

G. M. Pierantozzi,[1,*] S. Modesti,[2,†] M. Perlangeli,[3] R. Cucini,[1] S. Fiori,[4] F. Salvador,[1] G. Rossi,[5,1] and G. Panaccione[1]

[1]*CNR - Istituto Officina dei Materiali (IOM), S.S. 14 km 163.5, I-34149 Trieste, Italy*

[2]*formerly at Dipartimento di Fisica, Università di Trieste, I-34127 Trieste, Italy*

[3]*Laboratoire de Physique de la Matière Condensée, CNRS, Ecole Polytechnique, Institut Polytechnique de Paris, 91120 Palaiseau, France*

[4]*Catalan Institute of Nanoscience and Nanotechnology (ICN2), CSIC and BIST, Campus UAB, Bellaterra, 08193 Barcelona, Spain*

[5]*Dipartimento di Fisica, Università di Milano, I-20133 Milano, Italy*

(Received 14 February 2026; revised 21 July 2026; accepted 13 August 2026; published 25 August 2026)

We investigate the transient response to photodoping of Sn/Si(111)-($\sqrt{3} \times \sqrt{3}$) R30°, a simple and prototypical two-dimensional Mott-Hubbard insulator with a small gap on a triangular lattice, by time- and angle-resolved photoemission with a 120 fs time resolution. A transient metallic state forms nearly instantaneously after photoexcitation and persists for a few hundred femtoseconds, consistent with theoretical predictions and previous studies of small-gap Mott systems in one and three dimensions. The temperature dependence of the doublon lifetime indicates that the dominant relaxation mechanism involves coupling between charge and spin degrees of freedom. On a longer timescale, a small energy shift of the lower Hubbard band persists for more than 1 ns. We attribute this long-lived modification to energy renormalization of the Hubbard bands induced by the photoexcited electron-hole plasma in the Si substrate. Our results further demonstrate that substrate excitations and the dynamics of the three-dimensional electron-hole plasma play a significant role in ultrafast studies of two-dimensional materials supported on semiconducting or insulating substrates, while also pointing to a possible route for controlling transient electronic states.

DOI: 10.1103/bc4t-fzc3

I. INTRODUCTION

Photo-excited Mott insulators (MIs) may host emergent correlated phases inaccessible at equilibrium and absent in excited band insulators, including η-pairing superconductor, nonthermal spin and orbital orders, and unconventional charge-density-wave states predicted by many-body calculations [1–10], provided that the thermalization time is sufficiently long. The relevant thermalization timescale depends on the interaction strength and on short-range spin correlations. Strong local interactions (large Hubbard gaps) are expected to generate a thermalization bottleneck, allowing nonequilibrium states and making them experimentally observable, whereas weaker interactions (small Hubbard gaps) may instead lead to ultrafast thermalization that obscures distinct transient phases [1,9]. In the latter case, photoexcitation is expected to produce transient hot correlated bad-metal states, generally characterized by electronic temperatures far exceeding those accessible at equilibrium. Anyway, tracking the dynamics of such photoexcited states can provide valuable insight into the coupling between charge and low-energy degrees of freedom (spin, orbital, and lattice), as well as into the behavior of correlated electrons at high electronic temperature.

Photodoping creates low-energy excitations by generating doublons (doubly occupied sites) and holons (empty sites) in the Hubbard bands. In some cases, the resulting changes in the screened local interaction and exchange coupling can induce a partial or complete collapse of the Hubbard gap, accompanied by shift and broadening of the Hubbard bands [1–9], thereby driving an almost instantaneous insulator-to-metal transition. In time-resolved photoemission, this process manifests itself as spectral weight above the Fermi level (E_F) associated with photoexcited doublons in the modified upper Hubbard band (UHB), spectral weight at E_F if the Hubbard gap collapses, and changes in position and line shape of the lower Hubbard band (LHB).

Time-resolved photoemission and optical studies have revealed the photoinduced ultrafast insulator-to-metal transition in 1D MIs [11], organic MIs, and undoped cuprates [12] provided evidence for light-induced superconductinglike states in cuprates [13–15], iron-based compounds [16], correlated organic materials [17,18], and investigated the dynamics of photoexcited states in several three-dimensional Hubbard systems [15,19–21]. These dynamics, generally much faster than those of band insulators, are governed by the interplay between the on-site Coulomb repulsion U, the hopping energy t_h, the energy gap W, and the exchange interaction J [22].

*Contact author: pierantozzi@iom.cnr.it

†Contact author: smodestis1@gmail.com

In UO_2, a MI with a large gap ($W = 2.3$ eV) and large U (4.6 eV), photoexcitation does not induce detectable spectral weight at E_F, the LHB remains essentially unchanged, and the excited carriers exhibit a lifetime of a few picoseconds [23]. These excitations are thought to form Mott excitons (doublon-holon pairs bound by spin excitations) or polaronic excitons. Similarly, the gap remains open in another wide-gap MI, α-$RuCl_3$ ($W = 2$ eV, $U = 4$ eV), where doublons have lifetimes shorter than 200 fs and evolve into Mott excitons with lifetimes exceeding 500 ps [24]. In these large-U materials, the screening of the on-site Coulomb repulsion by photoexcited carriers is generally insufficient to perturb the gap. Moreover, inter-Hubbard-band thermalization is relatively slow because the gap energy is much larger than the energies of the available bosonic excitations (spin waves, phonons, and plasmons) [1]. In contrast, in cuprates such as Nd_2CuO_4 and La_2CuO_4 ($U > 2$ eV), photoexcitation induces a transient metallic state which decays in less than 200 fs, leaving behind localized carriers with lifetimes of several tenths of ps [12].

In systems with $U \leqslant 2$ eV and $W < 0.7$ eV, photoexcitation leads to a partial filling of the Mott gap on a timescale shorter than the experimental resolution (typically 10–100 fs). The lifetime of the transient metallic states differs substantially among materials, ranging from ~0.7 ps in 1T-TaS_2 [19–21] and 1.7 ps in V_2O_3 [25] to more than 400 ps in $V0_2$ [26]. The formation of a continuum of in-gap states is accompanied by a substantial intensity reduction of the LHB spectral weight and a pronounced modification of its line shape in 1T-TaS_2 [19–21,27]. In Sr_2IrO_4, a MI with U in the range 1–2 eV and $W \simeq 0.2$ eV, intraband cooling occurs in less than 70 fs, followed by a transient metallic state that persists for about 1 ps and subsequently evolves into an exciton fluid that lasts for a few picoseconds [28,29]. In this class of materials, the lifetime of photoexcited carriers in the upper Hubbard band is consistently short, ranging from less than 100 fs [19,28] to 200–300 fs [20,21,26,27]. This behavior is generally attributed to the strong coupling of doublons to spin degrees of freedom, which enables efficient relaxation through the emission of multiple magnetic excitations [22]. The doublon lifetime has been predicted to exhibit a strong temperature dependence owing to the loss of spin correlation at elevated temperatures [6]; however, to our knowledge, this effect has not yet been investigated experimentally in solid state MIs. The observed in-gap states and the pronounced modifications of the LHB in these MIs are reproduced by many-body model calculations [4,6,20,21,26,30]. These features are generally attributed to the substantial enhancement of low-energy dynamical screening, even at excitation densities of a few percent of an electron per unit cell [26], and to the nearly instantaneous quenching of the exchange interaction [7]. More generally, these systems are not expected to relax into long-lived nonthermal states but rather to thermalize rapidly into hot bad-metal states characterized by elevated electronic temperatures [1].

In this work, we experimentally investigate a small-gap quasi two-dimensional Mott-Hubbard system on a triangular lattice. Some triangular lattices of covalently bonded adatoms on semiconductor surfaces constitute structurally simple model systems for exploring the rich physics emerging from the interplay between Mott-Hubbard correlations,

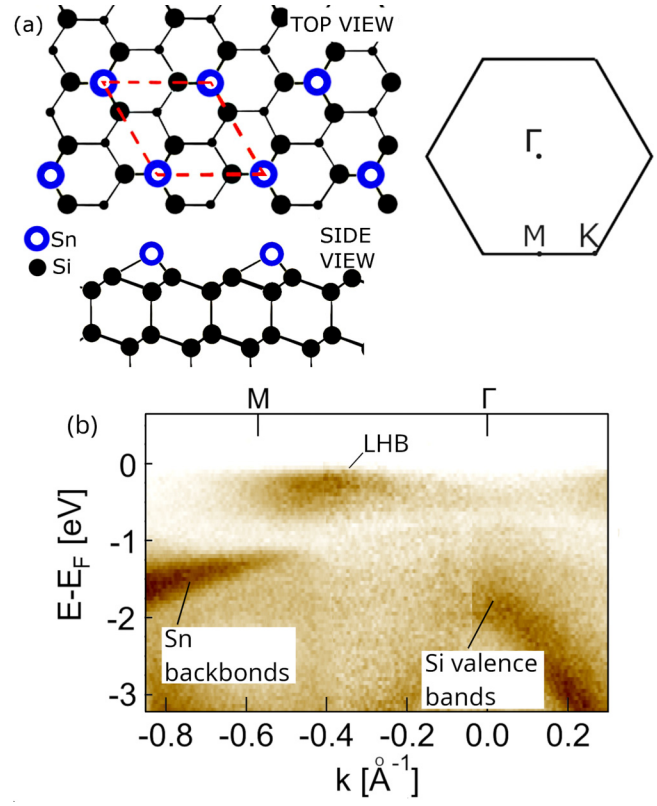

FIG. 1. (a) Schematic structure of the Sn/Si(111)-($\sqrt{3} \times \sqrt{3}$) R30° surface, with the unit cell outlined by red dashed lines. The surface Brillouin zone is shown on the right. (b) Photoemission intensity distribution map of the surface measured along the ΓM direction with h$\nu = 21.7$ eV and p polarized light. The lower Hubbard band (Sn p_z states hybridized with Si valence-band states) is at about –0.26 eV near M and at –0.35 eV at Γ, the Sn-Si backbond bands are centered at –1.2 eV, while the Si valence bands are below –1.5 eV.

geometric frustration, magnetism, superconductivity, charge ordering, and doping. A prototypical example is provided by one-third of a monolayer of Sn on the Si(111) surface in the Sn/Si(111)-($\sqrt{3} \times \sqrt{3}$) R30° structure (hereafter denoted $\sqrt{3}$), which realizes a quasi-two-dimensional single-band Mott insulator on a triangular lattice. This system undergoes a metal-insulator transition as a function of doping and temperature [31–35] and exhibits unconventional superconducting and pseudogap phases upon doping [34–37]. Sn/Si(111)-$\sqrt{3}$ shares several key features with the cuprates, including the parent Mott-Hubbard state, the strong effect of doping, and the emergence of unconventional superconducting and pseudogap phases upon doping. At the same time, it is structurally and electronically much simpler. The two-dimensional unit cell, which contains a single Sn adatom covalently bound to the three underlying Si atoms [Fig. 1(a)], is sufficiently simple to be treated by state-of-the-art many-body calculations with parameters derived entirely from *ab initio* simulations. These calculations successfully describe both the electronic structure of the parent MI and the superconducting phase that emerges upon doping (see Refs. [32,35] and Supplemental Material of Ref. [34]) and could, in principle, be extended to investigate the nature and dynamics of the photoexcited states. Sn/Si(111)-$\sqrt{3}$ hosts surface Hubbard bands within

the energy gap of the Si substrate [Fig. 1(b)], with $U \sim 0.7$ eV, $t_h = 50$ meV, $J = 3$ meV, a transition temperature of about 100 K, and a gap $W \sim 50$ meV [31,33], substantially smaller than that of $1T$-TaS_2. Unlike $1T$-TaS_2, its MI state is not intertwined with a charge density wave (CDW) phase, although it is predicted to be close to a transition into a CDW state [38]. Furthermore, many-body calculations based on *ab initio* estimates of the electron-phonon coupling predict a strongly nonlinear relaxation mechanism, which could lead to unusually long lifetimes of the photoexcited states [39].

We measured the time evolution of the photoexcited Sn/Si(111)-$\sqrt{3}$ MI by time- and momentum-resolved photoemission spectroscopy at sample temperatures of 30 K and 200 K, focusing on the formation, features, and lifetime of the transient metallic phase and the subsequent dynamics. Moreover, we investigated the role of the spin degree of freedom in the doublon relaxation process through the temperature dependence of the excitation lifetime, as well as the noticeable influence of the substrate excitations on the dynamics of this quasi-2D system. Interactions with the substrate may provide a route for manipulating the transient state of the overlayer, for instance, through the injection of photoexcited carriers or additional screening by the electron-hole plasma photogenerated in the substrate. This issue is of broad relevance for the investigation and possible exploitation of the ultrafast phenomena of other monolayerlike systems supported on insulators or semiconductors.

II. EXPERIMENTAL

The experiments were performed at the NFFA-Sprint [40] laboratory at CNR-IOM, Trieste. The *n*-doped Si(111) substrate (resistivity 0.002 Ω cm) was cleaned by repeated flashing to temperatures above 1500 K. One-third of a monolayer of Sn was deposited onto the substrate held at 550 °C. Low-energy electron diffraction confirmed the formation of a well-ordered $(\sqrt{3} \times \sqrt{3})$ R30° surface structure, with no evidence of the additional $2\sqrt{3} \times 2\sqrt{3}$ phase that develops at higher Sn coverages.

Equilibrium and time-resolved ARPES spectra were acquired by a Scienta SES 2002 hemispherical analyzer with ±6° acceptance. The polar rotation of the sample manipulator allows further exploration of the full Brillouin zone along the analyzer momentum dispersion. The laboratory is equipped with a pair of twin and jitter-free Light Conversion PHAROS lasers with tunable repetition rate and photon energy of 1.2 eV, which are used to seed, respectively, the probe and pump ultrafast beams. The probe is produced by a high harmonic generation (HHG) setup [41]: In this work, we employed a photon energy of 21.7 eV in *p* polarization (to exploit the favorable matrix element in the case of the investigated electronic states) with a photon energy resolution of 20 meV and a total energy resolution of 100 meV for the setting used in this study. The energy-tunable pump is instead generated by an optical parametric amplifier by Light Conversion with transform-limited time compression: In this experiment, the energy was set to 1.55 eV, *s* polarized. The spot diameter at normal incidence, measured exploiting a yttrium aluminum garnet crystal at the sample position, was 100×100 μm for the HHG beam, and 350×400 μm for the pump beam. The resulting fluence employed in the pump-probe experiments, except when noted, was around 0.8 mJ/cm^2 for the measurements at the *M* point (0.6 mJ/cm^2 at the Γ point, due to different incidence angle when working at different polar angle of the manipulator). These fluence values are below the threshold at which detectable space-charge effects are generated. The repetition rate employed in this experiment was 50 kHz and the time resolution estimated in previous experiments as the cross-correlation of the pump and probe pulses is 120 fs (110 fs for the probe and 50 fs for the pump). The position of the Fermi level with respect to the Hubbard band was established from static room-temperature measurements, where the surface photovoltage (SPV) effect is negligible, and independently validated at low temperature through comparison with published data acquired under similar experimental conditions [31,42]. The uncertainty in the Fermi-level position at 30 K is estimated to be ±20 meV. Scanning tunneling spectroscopy measurements were performed using a homebuilt scanning tunneling microscope.

Since the Sn adatoms are adsorbed on a semiconductor surface, their photoemission spectra are affected by the SPV [43] and Dember [44] shifts, as well as the associated broadening, induced by the pump pulse. The energy broadening arises primarily from spatial inhomogeneities in the pump fluence and in the surface-defect density. Owing to the mechanism discussed in Ref. [45], these effects influence the spectra for hundreds of picoseconds before and after the arrival of the pump pulse. For brevity, the combined contribution of the SPV and Dember effects and shifts will hereafter be referred to simply as the SPV effect and SPV shift.

In addition to the transient electric field associated with the SPV effect between the sample surface and the analyzer, changes in the binding energy of the surface states may also contribute to the time-dependent energy shift. The rapid variation in density of the photoexcited carriers at the surface and in the subsurface region modifies the many-body renormalization of electronic states on timescales comparable to the pump duration. A key difference between these two classes of effects is that the SPV-induced shift is temporally broadened and spread over hundreds of ps by the mechanism described in Ref. [45], whereas the renormalization-induced shift is not associated with an electric field extending outside the sample and is therefore not subject to this temporal broadening.

The time dependence of the energy shift arising from the effects discussed above was estimated as described below. The data presented here have been corrected for the energy shift, but not for the possible extrinsic SPV broadening caused by the spatial inhomogeneity in the pump fluence and the surface-defect density. The full width at half maximum of this extrinsic broadening is estimated to be approximately 60 meV by comparing the high-energy tail of the spectra acquired in the absence of the pump pulse with those measured 1 ps before the arrival of the pump pulse.

III. RESULTS

A. Shifts unrelated to Mott-Hubbard physics

To disentangle the effects arising from photodoping of the Mott–Hubbard state from those associated with surface

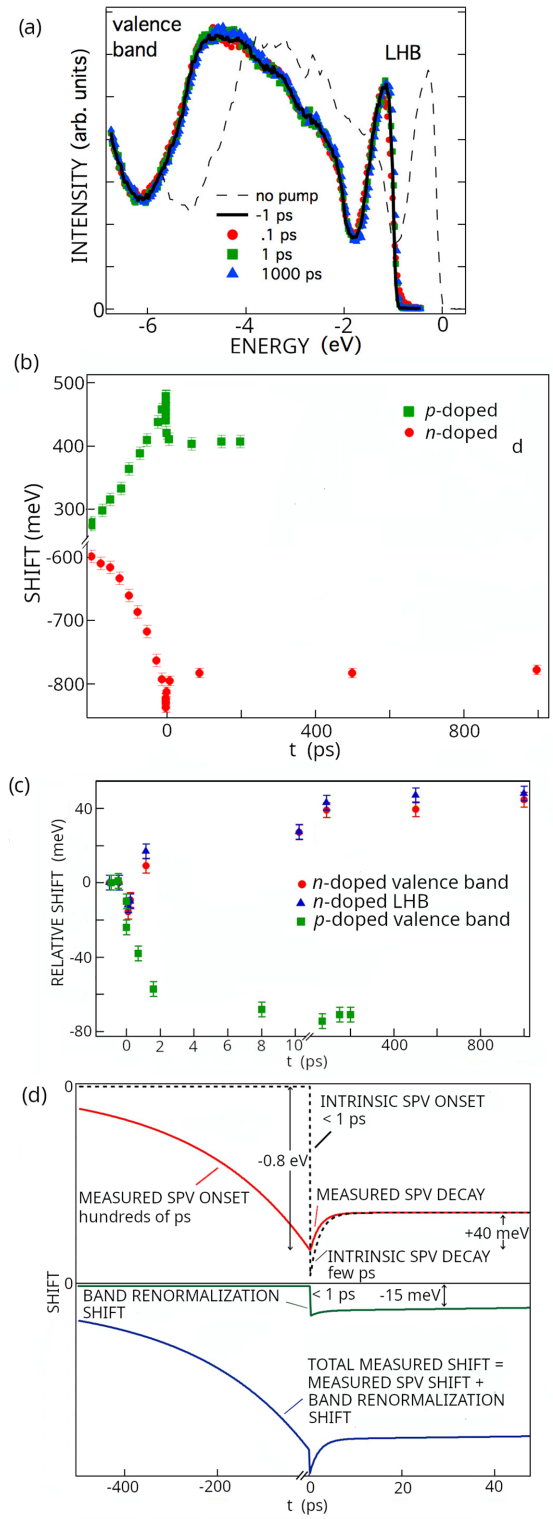

FIG. 2. (a) Photoemission spectra of the Sn/Si(111)-$\sqrt{3}$ surface measured at 30 K along the Γ-*M* direction and integrated from 0.2 to 0.8 Å^{-1}. The spectra were acquired with the pump blocked, 1 ps before the pump pulse, 0.1, 1, and 1000 ps after the photoexcitation, to evaluate energy shifts associated with the SPV and Dember effects. The pump fluence was 0.8 mJ/cm^2. (b) Energy shift of the valence-band spectrum relative to the unpumped spectrum evaluated in the binding-energy range between 1 and 6 eV, as a function of the delay t for *n*-doped (red circles) and *p*-doped (green squares) Si substrates. (c) Energy shifts of the valence band (*n*- and *p*-doped substrates) and of LHB (blu triangles, *n*-doped substrates) after photoexcitation, relative to their values 1 ps before the pump pulse. (d) Schematic illustration of the SPV and renormalization shifts. The shifts are not drawn to scale to enhance the visibility of the smaller contributions. Note the different time scales used for negative and positive pump–probe delays t.

photovoltage and energy renormalization processes discussed in the previous section, we measured the temporal evolution (as a function of the pump–probe delay t) of the shift of the photoemission spectral features associated with the valence band of the Si substrate and the Sn–Si backbonds (binding energy range 1–6 eV) at 30 K [see Fig. 2(a)]. The LHB, located approximately 0.26 eV below E_F, is well separated from the Si valence states in the momentum range $0.2 < k < 0.8$ Å^{-1} along the ΓM direction, where the spectra were acquired [31,32] [see Fig. 1(b)].

The rigid shifts were quantified by minimizing the least-squares residual between the valence-band spectrum at pump-probe delay t and the pump-off spectrum as a function of the energy shift between them. The resulting time-dependent shifts for both *p*- and *n*-doped substrates are shown in Fig. 2(b). The spectra on the *n*-doped substrate [red dots in Figs. 2(b) and 2(c)] before the pump pulse (negative delays t) show the large (about –0.8 eV) SPV-induced shift typical of semiconductor surfaces, which evolves slowly with time, as discussed in Ref. [45]. As discussed in the experimental section, the slow dynamics at negative delays arise from the electric field between the sample surface and the electron analyzer during the photoelectron flight-time (∼1 ns). This field broadens the much faster rise of the intrinsic SPV shift, which occurs on timescales of 1 ps or less [46–48]. Consistent with an SPV-driven mechanism, the shift at negative delays reverses sign on *p*-doped substrates [Fig. 2(b), green squares].

A sudden shift of -15 ± 4 meV occurs upon pump excitation ($t = 0$) within 0.5 ps on both *n*-doped and *p*-doped substrates [see Fig. 2(c)]. Due to its nearly instantaneous onset, this jump at $t = 0$ cannot be attributed to processes like the SPV effect, which produce electric fields extending into the vacuum outside of the sample; if it were, the mechanism described in Ref. [45] would have broadened and distorted the transient. Furthermore, because the shift's sign is independent of bulk doping, it cannot be linked to band-bending effects. Instead, it originates from the band renormalization driven by the high density of photo-excited carriers in the subsurface regions.

A pump pulse at 1.55 eV (fluence: 0.8 mJ/cm^{-2}) generates an electron-hole plasma in the subsurface Si with a density of approximately 10^{19} cm^{-3}, given the Si absorption coefficient of 10^3 cm^{-1} at this energy. This plasma induces a sudden renormalization of the Si band energies by tens of meV [49], occurring within our time resolution. Similar plasma-induced renormalization (∼10 meV) has been observed on the clean Si(111)-7 × 7 surface on subpicosecond timescales [50]. This renormalization is also expected to affect the Hubbard bands, owing to the hybridization between the Sn p_z states and the Si valence-band states [32]. However, the renormalization of the Hubbard bands may differ from the renormalization of the

valence band. Since the plasma lifetime in Si exceeds 1 ns [51], the associated renormalization shift is expected to persist on comparable timescales.

The abrupt drop at $t = 0$ is followed at positive delays by a tens-of-meV energy shift with a few-picoseconds time constant [Fig. 2(c)]. Since this slower component reverses sign between *n*-doped and *p*-doped substrates, we attribute it to the partial decay of the SPV induced by a rapid redistribution or partial recombination of the free carriers near the surface. Surface defects may accelerate this decay relative to the plasma lifetime in the bulk. The effect reported in Ref. [45] does not modify the time constant of the exponential SPV decay at positive delays but substantially reduces its amplitude. Indeed, energy shifts on a ∼1 ps timescale, attributed to the rapid decay of the SPV, have already been observed on GaAs and GaP surfaces following photoexcitation [46–48]. A schematic illustration of the shifts discussed above for an *n*-doped Si substrate is shown in Fig. 2(d), where the SPV shift and the band-renormalization shift are represented separately. The band-renormalization contribution is expected to decrease gradually following the decay of the electron-hole plasma density. In a *p*-doped sample, the SPV shift reverses sign, whereas the band-renormalization shift remains negative.

Figure 2(c) also compares the time-dependent shift of the midpoint of the high-energy side of the LHB (blue triangles) with that of the valence band (red dots) for *n*-doped subtrate. Because these shifts are similar, the combined SPV and renormalization shifts of the LHB are approximately comparable to those of the deeper Si valence states. Notably, after the pump pulse, the LHB shift is offset from that of the valence band by ∼10 meV. In summary, the comparison between *n*- and *p*-doped substrates reveals that the temporal evolution of the spectral shifts, including that of the lower Hubbard band, are driven by the SPV effect at times $t < 0$ ps and $t > 0.5$ ps. Conversely, band renormalization dominates the dynamics within the first 0.5 ps following the pump pulse.

B. Time evolution of the Hubbard bands and gap filling

In the following, all spectra have been measured on an *n*-doped Si substrate and corrected by subtracting the time-dependent energy shift of the Si valence band discussed in the previous section. The energy scale is referenced to the Fermi-level position measured 1 ps before the pump pulse. Since the plasma-induced energy renormalization is ∼15 meV and is substantially taken into account by our correction procedure, we assume that the Fermi-level position does not significantly change after photoexcitation.

The time evolution of the LHB and of the spectral region above E_F is shown in Figs. 3(a) and 3(b) with logarithmic and linear intensity scales, respectively. Time-resolved photoemission spectra were acquired at 30 K near the *M* point along the Γ–*M* direction in reciprocal space [52].

Within a few hundred femtoseconds after the arrival of the pump pulse, the spectral intensity increases in the energy window from −0.1 to ∼0.4 eV around and above E_F [Fig. 3(a)], while the intensity at the top of the LHB is reduced by ∼10% [Fig. 3(b)]. This attenuation is prominent at the surface Brillouin-zone edge and absent near Γ, where the band lies ∼0.1 eV deeper (see Appendix 1). Above E_F, the spectral intensity decays approximately exponentially with energy, corresponding to an effective electronic temperature of order of 1000 K at $t = 0$ [Fig. 3(a)]. After ∼1 ps, the spectral intensity above E_F falls to the noise level, while the LHB recovers its full peak intensity [Fig. 3(b)].

The LHB spectra measured from 1 ps up to 1 ns after photoexcitation remain broadly similar to the prepump spectrum ($t = -1$ ps), apart from an upward shift of ∼10 meV [Fig. 3(b) and Appendix 2]. As discussed in the Appendix, the long-delay LHB line shape shows weak indications of a residual modification with respect to the prepump shape, although the observed differences are comparable to the experimental uncertainty. Together with the ∼10 meV energy shift, this suggests the presence of small but persistent modifications of the Hubbard states.

The time dependence of the temperature of the excited carriers was extracted by fitting the photoemission spectra above the Fermi level with a Fermi-Dirac distribution [Fig. 3(c)]. These values represent a first-order approximation, as the density of states (DOS) deviates significantly from a constant value: specifically, it exhibits a minimum near E_F and a maximum 0.5 eV above E_F [31–37], leading to an estimated temperature uncertainty of 100 K. Within 1 ps, the electronic temperature decreases from about 1000 K to values below 400 K, the latter being the measurement limit imposed by the SPV broadening.

Under the assumption of a constant photoemission matrix element, the time-dependent DOS can be approximately estimated by dividing the photoemission spectra by a Fermi-Dirac distribution at the corresponding electronic temperature. This method is reliable only when the thermal broadening at high energy exceeds the extrinsic broadening due to surface photovoltage and the instrumental resolution, i.e., in the time window –0.2 to 0.5 ps. The results [Fig. 3(d)] reveal the prompt rise of the high-energy tail of the LHB, which partially fills the Mott gap, together with the transient emergence of the UHB at about 0.4 eV above E_F. The latter is observed both near *M* and Γ [Fig. 3(e)] and provides direct evidence for the photoinduced doublon population.

It is interesting to compare the reconstructed DOS of the transient state at $t = 0$ with the equilibrium DOS of the same system in the high-temperature metallic phase at 300 K, obtained by photoemission spectroscopy [31] and scanning tunneling spectroscopy, as shown in Fig. 3(f). The DOS minimum in the transient photoexcited phase is shifted by more than 0.1 eV toward higher energy relative to the equilibrium 300 K metallic phase, while remaining deeper despite the much higher electronic temperature. This suggests that the transient state cannot be described as a simple high-temperature metallic phase. The center of the transient UHB lies at slightly lower energy than that observed at equilibrium at low temperature by scanning tunneling spectroscopy (STS) [34–37] (about 0.5 eV), and close to that of the metallic phase at 300 K [Fig. 3(f)]. The exact positions of the DOS minimum and the UHB center depend on the temperature used to extract the DOS from photoemission data at $t = 0$. As discussed in Appendix 3, we used a temperature of 850 K to reconstruct the DOS, corresponding to the most conservative estimate of the DOS features. The actual position of the DOS minimum is expected to lie at higher energy, and the UHB at a lower

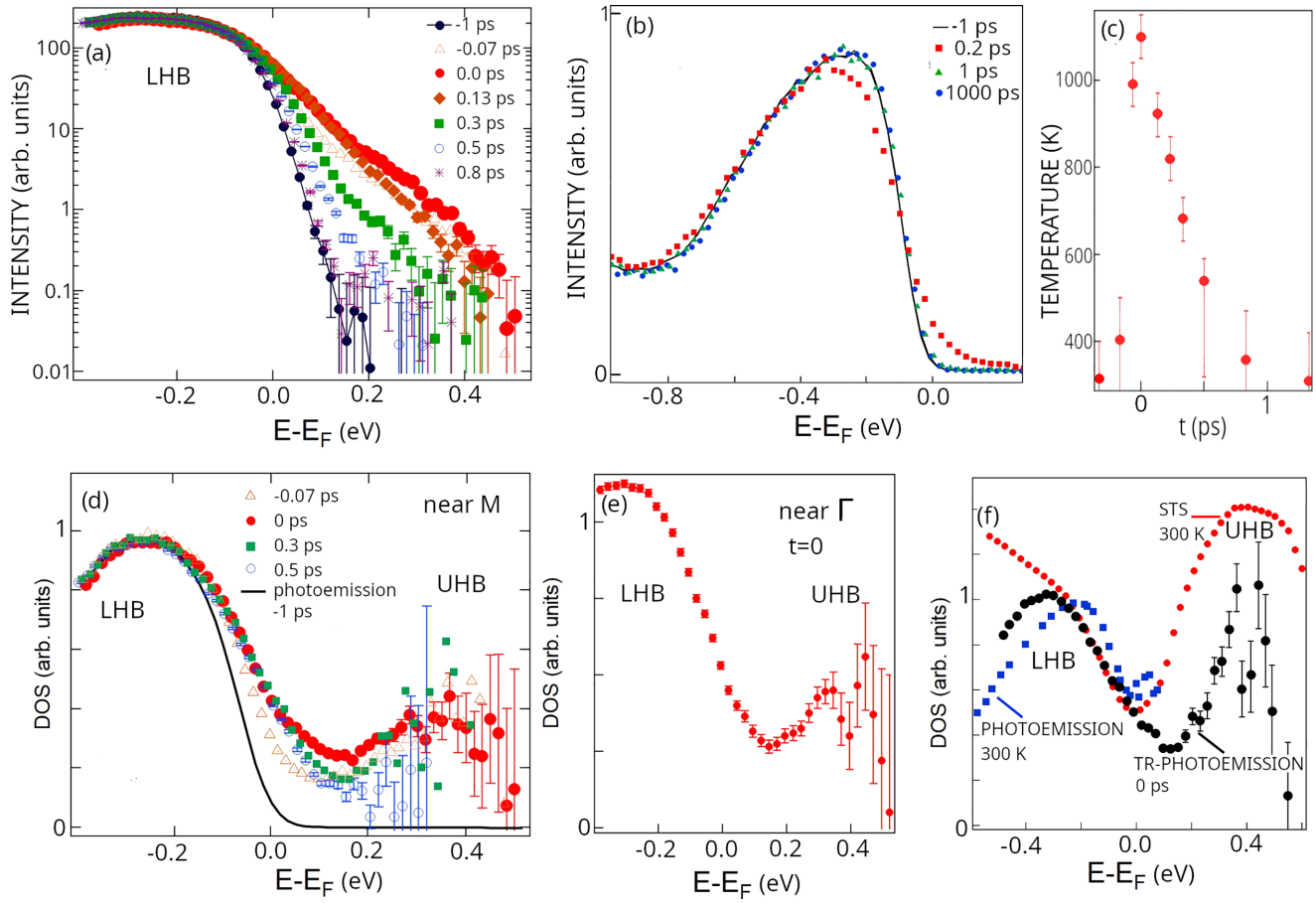

FIG. 3. (a), (b) Photoemission spectra of the Hubbard-bands region near the M point at different pump-probe delays on logarithmic and linear intensity scales, respectively. The substrate was n-doped. All the spectra have been shifted in energy according to the delay dependent values shown in Fig. 2(b). (c) Time dependence of the electronic temperature extracted from the photoemission spectra. (d) DOS near M at different times, estimated by dividing the photoemission spectra by a Fermi-Dirac distribution at the corresponding electronic temperature. The resulting DOS is compared to the photoemission spectrum before the arrival of the pump pulse (black line). (e) DOS near the Γ point at $t = 0$. (f) Total DOS of the photoexcited state (large black dots) compared to that of the equilibrium metallic state at 300 K obtained by photoemission (blue squares) and scanning tunneling spectroscopy at 300 K (small red dots). The DOS is reconstructed by summing the spectra measured at the M and Γ points and assuming an electronic temperature of 850 K.

energy, than shown in Fig. 3(f). Therefore, the differences between the transient and the equilibrium DOS are robust, even though the detailed profiles depend on the assumed electronic temperature.

Figure 4 shows the time dependence of the transient doublon population, evaluated from the spectral intensity of the UHB integrated in the 0.15–0.5 eV energy range. The transient trace measured at 30 K exhibits a FWHM (full width at half maximum) of 220 fs, exceeding the 120 fs FWHM of the pump-probe cross-correlation, which defines the experimental time resolution. By fitting the trace with a finite-rise-time peak followed by an exponential decay, convoluted with a Gaussian of 120 fs FWHM (instrumental resolution), we extract a doublon lifetime of 110 ± 20 fs. The fitted rise time is <30 fs. Notably, the same transient response measured at 200 K, where the system is metallic already at equilibrium, is substantially broader and corresponds to a longer UHB population lifetime of 200 ± 50 fs (Fig. 4).

Besides the doublon population, the time dependence of the spectral intensity at energies below the UHB allows us to extract the characteristic timescales of other transient processes. Figure 5(a) shows the false-color map of the transient differential photoemission intensity, obtained by subtracting the prepump spectrum at $t = -1$ ps from the spectra acquired at different pump-probe delays t, as a function of energy and t in the range from –1.2 to 1.8 ps. Fig 5(b) extends the delay range to 13 ps. Figures 5(c) and 5(d) show the time dependence of the spectral intensity at selected energies after subtraction of the pre-pump intensity. The spectral intensity at E_F [black triangles in Fig. 5(c) and 5(d)], associated with the Hubbard gap filling, rises rapidly and reaches its maximum on a timescale comparable to the temporal resolution of the experiment, decays initially with a time constant of about 0.36 ps, and then decreases more slowly, remaining above the prepump intensity at long delays. This residual intensity originates from the contribution of the upward shifted LHB. The persistent LHB shift also affects the spectral intensity at long delays at –0.1 eV (orange squares), where the signal increases over ∼0.5 ps and subsequently partially decays without reaching the prepump intensity. The nearly instantaneous suppression of photoemission intensity at $t = 0$ at –0.2 eV [blue circles in Fig 5(c)], close to the LHB maxi-

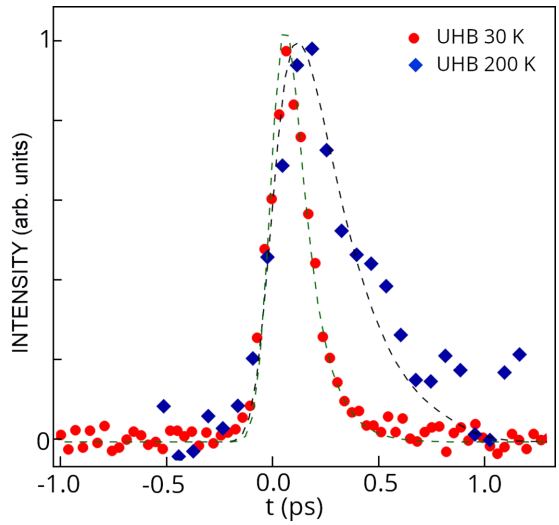

FIG. 4. Time dependence of the UHB photoemission intensity integrated from 0.15 to 0.5 eV measured at 30 K and at 200 K. The dashed curves are least-squares fits of the data using the function described in the text.

mum, is followed by a rapid recovery within a few hundred femtoseconds. At the Brillouin zone center, the photoemission intensities exhibit the same dynamics presented in Figs. 4 and 5(c) at E_F and above it. In contrast, the LHB peak intensity remains constant, differing from the dynamics observed at the other symmetry point (see Appendix 1).

IV. DISCUSSION AND CONCLUSIONS

In summary, after removing energy shifts affecting all bands, we identify ultrafast dynamics in the Hubbard bands on timescales ranging from 100 to 400 fs. These include the prompt rise of the doublon population in the UHB, followed by a rapid, temperature-dependent decay (100 fs at 30 K vs 200 fs at 200 K) (Fig. 4); the rise and subsequent decay (0.36 ps) of spectral weight at the Fermi level, in the Hubbard gap; and the fast suppression and recovery of the LHB peak intensity at the Brillouin-zone edge (within ∼300 fs) [Fig. 5(c)]. In addition, we observe a slower process, evidenced by a ∼10 meV shift of the LHB, persisting for hundreds of picoseconds [Figs. 2(c), 3(b), and 5(d)].

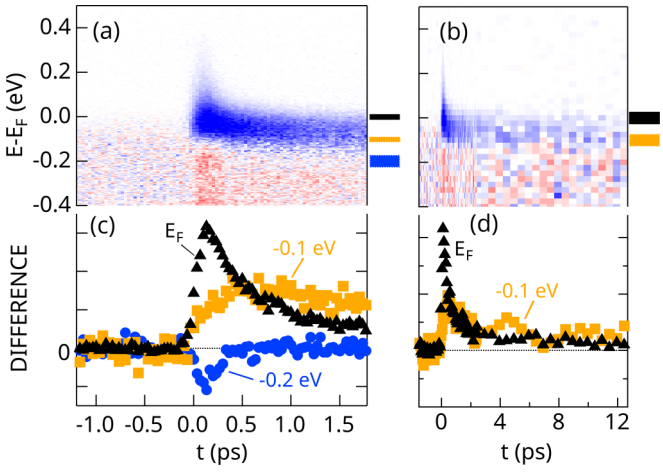

FIG. 5. (a), (b) False-color map of the transient differential photoemission intensity as a function of energy and pump-probe delay. Blue (red) regions correspond to an increase (decrease) of spectral intensity relative to the spectrum at $t = -1$ ps. (c), (d) Time dependence of the spectral intensity at selected energies (0.0, –0.1, and –0.2 eV) after subtraction of the prepump intensity.

A. Fast dynamics

The thermalization of the photoexcited doublons into a quasithermal distribution with an electronic temperature T is expected on a timescale of $h/2\pi W$, i.e., a few femtoseconds or tens of femtoseconds [6]. This is consistent with the nearly exponential energy dependence of the spectral intensity above E_F already at $t = 0$ [Fig. 3(a)]. Thermalization within the time resolution has also been reported in $1T$-TaS_2 [19–21,27].

The doublon decay time in our system ($W = 0.05$ eV, $U = 0.7$ eV, $t_h = 0.05$ eV, $J = 3$ meV) is expected to lie in the range 20–200 fs [22]. Although the spin-excitation energy scale is small ($J = 3$ meV), the gap is only on the order of tens of meV at 30 K, enabling efficient decay of doublons into multiple magnetic excitations. The measured lifetime (∼100 fs at low temperature) is consistent with the theoretical estimates and the values reported in other small-gap MIs, such as $1T$-TaS_2 and α-$RuCl_3$, where doublon lifetimes are <20 fs and 200 fs, respectively [19,24]. It is, however, significantly shorter than in large-gap Mott insulators such as UO_2, where lifetime is on the order of several picoseconds [23].

Notably, the doublon lifetime exhibits a strong temperature dependence, increasing by a factor of 2 between 30 K and 200 K (Fig. 4). This unusual trend is consistent with a decay mechanism dominated by spin-charge interactions, as previously proposed in Ref. [6]. The short-range spin correlations, which provide an efficient dissipation channel for doublons in the MI phase at 30 K, are strongly suppressed in equilibrium above 70 K, where the system enters the bad-metallic phase [31]. Although the high electronic temperature reached during the first 100 fs after photoexcitation is expected to further weaken the spin correlations, they are likely to remain stronger when the system is initially a MI than when it is a bad metal. Charge excitations across the Fermi level represent a possible alternative decay channel. However, this hypothesis is inconsistent with the observed temperature dependence: If this channel were dominant, the lifetime at 200 K (where the equilibrium state is already metallic) would be shorter than at 30 K (where the equilibrium state is insulating). Furthermore, a decay pathway mediated by electron-phonon interactions is again inconsistent with the observed thermal trend. Such interactions typically lead to a reduction in lifetime at elevated temperatures due to the increased phonon population [53]. Therefore, to our knowledge, the spin-charge interaction is the only decay channel that explains the temperature dependence of the lifetime.

Photoinduced modifications of LHB are predicted to occur on a timescale of $h/2\pi t_h$ (i.e., a few femtoseconds in our case) [9,30] and have been observed on a timescale of tens of fs [27]. In Sr_2IrO_4, in-gap states emerge within the instrumental resolution (60 fs) [28]. This rapid response is consistent with

the appearance of in-gap states within the temporal resolution of the experiment [Figs. 3(d)–3(f)], as evidenced by the prompt increase in spectral intensity at E_F [black triangles in Fig 5(c)]. Such an increase cannot simply be accounted for by an elevated electronic temperature, which would broaden the Fermi-Dirac distribution without generating additional spectral weight at E_F. Therefore, it indicates an enhancement of the density of states near the Fermi level.

The transient metallic states at E_F decay with a time constant of ∼0.36 ps [black triangles in Fig. 5(c)]. Similar photoinduced metallization within the experimental time resolution has been observed in other small gap MIs, including V_2O_3, Sr_2IrO_4, a-$RuCl_3$, and 1T-TaS_2. In these systems, however, the lifetime of the metallic state is longer than in Sn/Si(111)-$\sqrt{3}$, ranging from about 0.7 ps in Sr_2IrO_4 to 1.7 ps in V_2O_3 [19–21,24,25,28,29]. In 1T-TaS_2, the increase in spectral intensity at and above E_F (UHB) and the corresponding depletion below E_F (LHB) is nearly one order of magnitude larger than those observed here, even at pump fluences four times lower than those used in our experiment [19–21]. While this difference could be attributed to a substantially larger optical absorption coefficient at the pump energy of 1T-TaS_2, it should also be noted that the nature of the insulating state of 1T-TaS_2 remains under debate [54] and is intertwined with a CDW phase, implying comparable electron-electron and electron-phonon interaction strengths. In contrast, no experimental evidence of strong electron-phonon coupling has been reported for Sn/Si(111)-$\sqrt{3}$; on the contrary, this coupling is predicted to be unusually weak [39]. Another material exhibiting markedly different behavior is VO_2, where the photoinduced metallic state persists for more than 400 ps, likely due to the strong coupling to the lattice associated with the structural component of the metal-insulator transition [26].

An interesting aspect is the difference between the DOS of the transient metallic state near $t = 0$ and that of the same system in the equilibrium bad-metallic phase at 300 K [Fig. 3(f)]. In the transient state, the DOS minimum near E_F is both deeper and shifted toward higher energy. A similar displacement of the minimum above E_F is also visible in transient spectra of 1T-TaS_2 reported in Ref. [19] [Figs. 1(b) and 2(a)]. Interestingly, the shift and asymmetric shape of the minimum are common features of spectral functions obtained in several many-body calculations for photoexcited Mott–Hubbard systems and for systems at elevated electronic temperatures [6,19–21,27]. The downward energy shift of the transient UHB with respect to its low-temperature equilibrium position (0.5 eV) [34–37] is expected as a consequence of the transient reduction of the effective correlation energy induced by the enhanced screening in the photoexcited state [1]. This effect has been reported in $LaBaCuO_4$ [55] and NiO [56] in agreement with the calculations of Ref. [30].

The LHB undergoes a distinct evolution at its maximum: At $t = 0$, the top of the LHB exhibits a sharp 10% decrease at the M point [blue circles in Fig. 5(c)], while remaining constant near Γ (see Appendix 1). We attribute this rapid suppression at M primarily to the elevated electronic temperature (about 1000 K) of the Fermi-Dirac distribution at $t = 0$. Specifically, compared to the distribution at 30K, the 1000 K distribution is reduced by approximately 10% at –0.2 eV, close to the LHB maximum at M, whereas it decreases by only 2–3% at –0.3 eV, where the LHB peaks at Γ. The elevated electronic temperature near $t = 0$ likely also contributes to the relatively slow increase of the spectral intensity at −0.1 eV [orange squares in Fig. 5(c)]. Even assuming an instantaneous increase of the DOS caused by in-gap states or an upward shift of the LHB, the reduced Fermi–Dirac occupation below E_F would partially compensate their effect on the photoemission intensity within the first few hundred femtoseconds, since the occupation probability at −0.1 eV is ∼0.7 at 1000 K.

B. Slow dynamics

The long-lived response to photoexcitation consists of a ∼10 meV upward shift of the LHB, which results in an enhanced spectral weight near E_F. We exclude the lattice heating induced by the pump pulse as the primary origin of LHB modifications, since the corresponding temperature increase is estimated to be less than 10 K at the fluence of 10^{-3} J cm^{-2} [57]. The lattice temperature therefore remains well below the metal-insulator transition temperature (∼70 K). Moreover, an increase in lattice temperature would broaden the LHB [31,42], in contrast to our observations. We attribute the persistent energy shift of the LHB primarily to the energy renormalization induced by the electron-hole plasma photogenerated in the Si substrate. Because the plasma in bulk Si persists for more than 1 ns [51], the resulting renormalization of the Si bands, of the order of tens of meV [49,50], is expected to survive on similarly long timescales. In our data, this renormalization is reflected in the ∼15 meV dip at $t = 0$ of the Si valence-band energy shown in Fig. 2(c). Since the Hubbard bands contain hybridized Sn p_z and Si valence-band states and lie within the Si gap [32], they are also expected to be affected by the plasma-induced energy renormalization, with an energy shift that may differ from that of the valence band. We attribute the ∼10 meV offset between the long-delay shifts of the LHB and the Si valence band (Fig. 2(c)) to the distinct renormalization experienced by the two states. Since the spectra shown here are corrected by subtracting the time-dependent energy shift of the Si valence band, including both the SPV contribution and the valence-band renormalization, the residual difference between the two renormalizations appears as an upward shift of the LHB by ∼10 meV at long delays.

The electron–hole plasma photogenerated in the substrate can also induce an additional shift of the LHB through a different mechanism. In particular, the SPV and the n-type doping of the substrate produce a large excess of holes in the Si subsurface region. Achieving flat-band conditions (corresponding to the observed 0.8 eV SPV shift), requires an excess hole density of the order of $10^{18} - 10^{19}$ cm^{-3}. Such a carrier concentration could induce p-type photodoping of the surface MI, analogous to chemical doping by B [34,35], thereby reducing the LHB $- E_F$ energy separation. However, within a simple rigid-bands picture, photodoping would be expected to shift the LHB and the valence band by comparable amounts, in contrast to the different shifts observed experimentally. We therefore conclude that photodoping alone is unlikely to account for the observed long-delay LHB shift

and attribute the dominant contribution to the plasma-induced energy renormalization.

For completeness, we briefly discuss two additional mechanisms proposed for the emergence of long-lived transient states in our system. Our present data do not allow us to determine whether these mechanisms contribute to the observed long-delay response. One possibility is anomalously slow electron–phonon relaxation in the Sn overlayer. Once a metastable phase is established through relaxation processes involving charge and spin degrees of freedom, its decay is expected to proceed primarily through coupling to phonons. However, according to Ref. [39], phonon-mediated relaxation is a highly nonlinear process in this correlated system and may occur on anomalously long timescales, extending up to hundreds of nanoseconds. In such a scenario, residual electronic heating could persist, which might contribute to a shrinking of the Hubbard gap and an upward shift of the LHB. A second possible origin of long-lived states is the slow recovery of spin correlations following the pump pulse. According to Ref. [58], magnetic dynamics in two-dimensional systems can evolve on timescales substantially longer than charge dynamics, suggesting that the recovery of short-range spin correlations may remain slow even after the electronic degrees of freedom have relaxed.

C. Conclusions

The response of Sn/Si(111)-$\sqrt{3}$ to ultrafast photodoping reveals both fast and slow dynamical regimes in a simple quasi-2D Mott-Hubbard system on a triangular lattice, free from competing phases. The fast dynamics, involving the doublon population and the transient gap filling on 100–400 fs timescales, are consistent with many-body calculations and similar to those observed in other small gap Mott-Hubbard systems and cuprates. The pronounced temperature dependence of the doublon lifetime in the UHB, with a counterintuitive increase of the lifetime upon increasing temperature, points to a relaxation mechanism governed by the coupling between charge and spin degrees of freedom, consistent with theoretical predictions. The slow dynamics, persisting for more than 1 ns, can instead be attributed to the long-lived, high-density electron-hole plasma photogenerated in the Si substrate, which renormalizes the energies of the Hubbard bands and of the Si valence band by different amounts.

More generally, our results show that energy shifts unrelated to intrinsic Mott physics can arise from photocarriers dynamics in the substrate. Similar effects may also occur in other insulating systems and supported quasi-2D materials and should therefore be considered in the interpretation of time-resolved spectroscopic measurements.

Regarding the proposed η-pairing phase, which has not yet been experimentally confirmed, Ref. [9] predicts that it should be more efficiently induced by excitations with photons energy significantly lower than that used in the present study. Time-resolved experiments investigating the ultrafast response as a function of pump-photon energy could therefore provide a route to detecting this phase, should it form in the Sn/Si(111)-$\sqrt{3}$ system. By varying the relative excitation densities in the surface layer and in the substrate, such experiments could help disentangle intrinsic Mott-Hubbard dynamics from substrate-induced screening and carrier-generation effects. For example, lower-energy (midinfrared) photons are expected to reduce the excitation density in the substrate, thereby minimizing the contribution of the photogenerated subsurface plasma. Another promising direction is the possible creation of metastable doped phases through the controlled injection of electrons or holes from photoexcited n- or p-doped substrate.

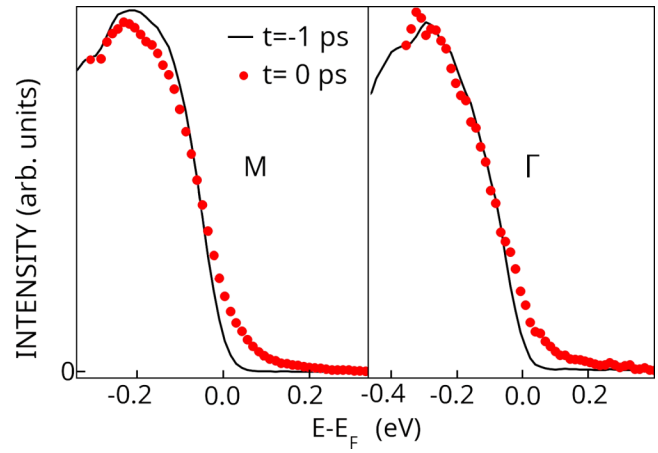

FIG. 6. Comparison between the photoemission spectra measured near the M and Γ symmetry points at 30 K before the pump pulse ($t = -1$ ps) and at $t = 0$.

ACKNOWLEDGMENTS

This work was performed in the framework of the Nanoscience Foundry and Fine Analysis (NFFA-MUR Italy Progetti Internazionali) facility supported by Ministero dell' Università e della Ricerca (MUR) as the Activity of International Relevance NFFA [59].

DATA AVAILABILITY

The data that support the findings of this article are openly available [60].

APPENDIX

1. Momentum dependence of the transient spectral changes

Figure 6 shows the time-resolved photoemission spectra measured around the M and Γ symmetry points before photoexcitation ($t = -1$ ps) and at the maximum of the photoinduced response ($t = 0$ ps). The LHB at Γ lies about 0.1 eV deeper in energy than at M. Notably, its maximum intensity remains essentially unchanged near Γ, whereas a clear suppression is observed near M. The reduction of the spectral intensity is centered at about –0.2 eV and appears more pronounced at M than at Γ.

2. Long-lived shift of the lower Hubbard band

Figure 7 illustrates the upward energy shift of the LHB more clearly than Fig. 3(b) by comparing the time-resolved photoemission spectrum measured before photoexcitation

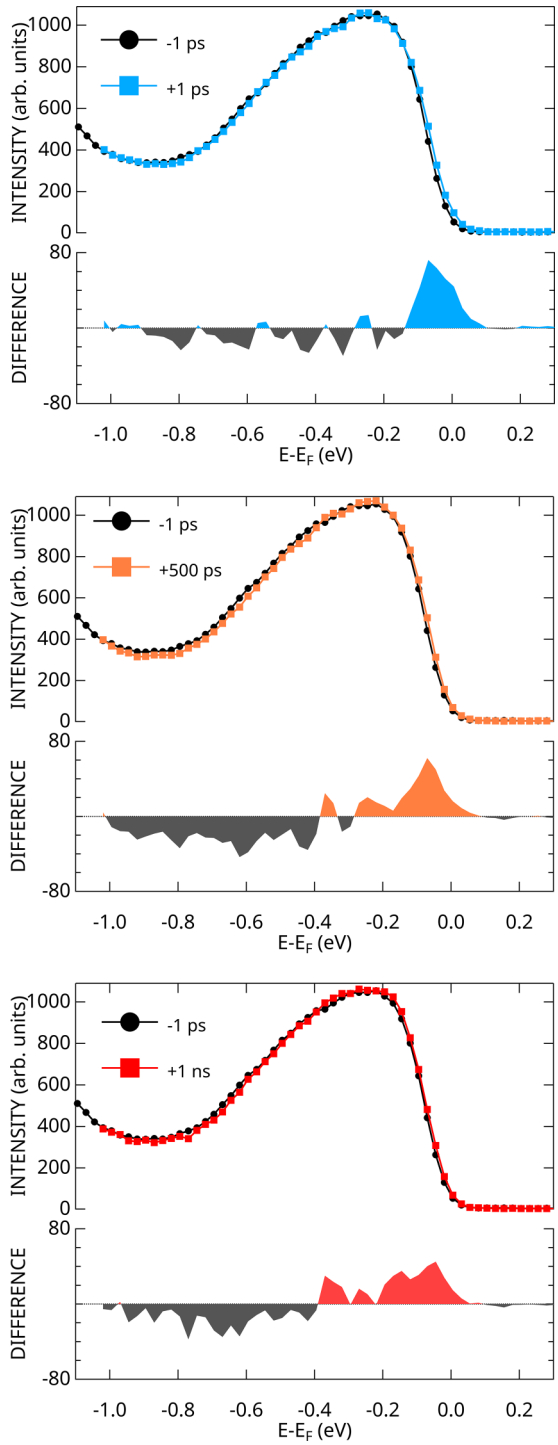

FIG. 7. Spectra of the LHB measured at delays of 1 ps, 500 ps, and 1 ns after photoexcitation compared with the prepump spectrum at $t = -1$ ps. The corresponding spectral differences with respect to the prepump spectrum are also shown. All spectra are corrected for the energy shift shown in Fig. 2(c) (see main text).

($t = -1$ ps) with those measured at 1 ps, 500 ps, and 1000 ps. The corresponding difference spectra, obtained by subtracting the $t = -1$ ps spectrum, are also shown. For the spectra at long delays, the difference is positive between the LHB maximum and the Fermi level and negative on the high-binding-energy side of the LHB, consistent with an approximately rigid upward shift of the LHB by about 10 meV.

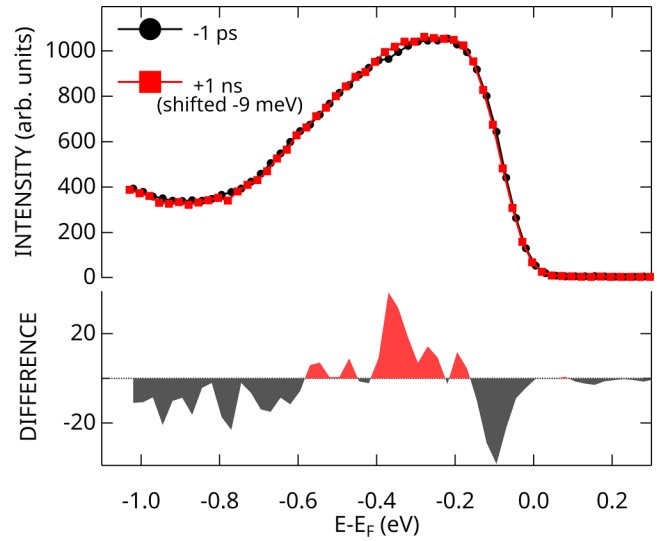

FIG. 8. Comparison between the prepump spectrum at $t = -1$ ps and the spectrum at $t = 1$ ns after energy alignment to minimize their difference. The residual spectral difference, shown at the bottom, is positive around the LHB maximum and negative on both sides of the peak.

Figure 8 compares the spectrum measured at $t = 0$ with that measured at 1 ns after shifting the latter downward in energy by an amount that minimizes the difference between the two spectra. The corresponding difference spectrum is also shown. Although the signal-to-noise ratio is limited, the difference tends to be positive near the LHB maximum and negative on both sides of the peak, suggesting a possible narrowing of the LHB at long delays.

3. Effect of the assumed electronic temperature on the reconstructed DOS

The DOS of the transient state at $t = 0$, shown in Fig. 3(f), was estimated by dividing the corresponding photoemission spectrum by a Fermi-Dirac distribution at 850 K. The electronic temperature carries a relatively large uncertainty (∼100 K), since it was extracted from a fit of the high-energy tail above E_F in an energy region where the DOS is not constant. An incorrect temperature introduces systematic errors in the reconstructed DOS. To assess the impact of this uncertainty on the energies of the DOS minimum and of the UHB maximum, Fig. 9 compares the DOS obtained using temperatures between 850 and 1200 K. The electronic temperature estimated at $t = 0$ is 1100 K [see Fig. 3(c)]. The lowest temperature considered, 850 K, represents the most conservative case, as it places the DOS minimum closest to E_F and the UHB maximum at the highest energy. Moreover, this temperature differs from the estimated value by more than twice the associated uncertainty. Even at this temperature, the DOS minimum remains above E_F and the UHB maximum remains below 0.5 eV. Increasing the temperature shifts the DOS minimum toward higher energies and the UHB maximum toward lower energies. Figure 9 demonstrates that,

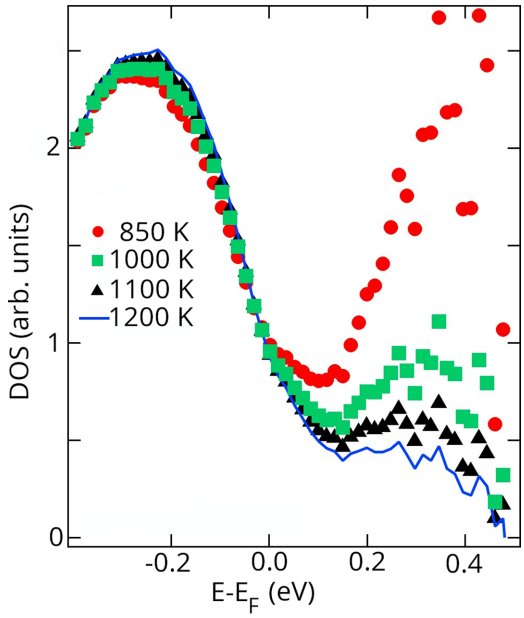

FIG. 9. DOS of the transient state at $t = 0$, reconstructed by dividing the time-resolved photoemission spectrum by Fermi-Dirac distributions with temperatures between 850 and 1200 K, illustrating the uncertainty associated with the electronic-temperature determination.

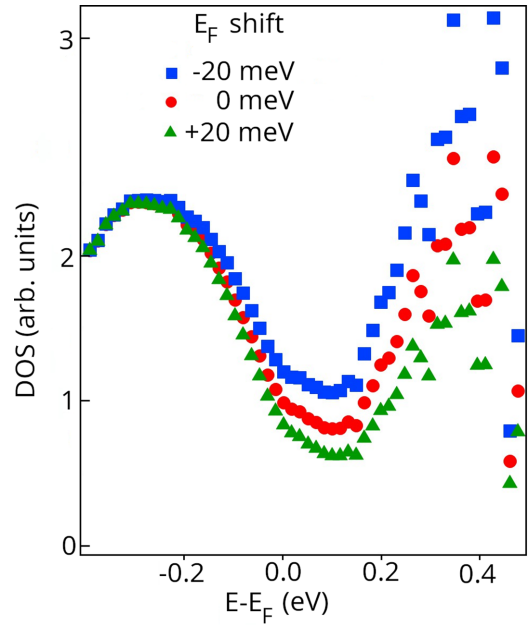

FIG. 10. Reconstructed DOS at $t = 0$ obtained using the Fermi-level position measured before the pump pulse (red dots) and using Fermi-level positions shifted by ±20 meV (blue squares and green triangles) to evaluate the effect of the uncertainty in E_F.

even over a temperature range substantially larger than the uncertainty in the estimated temperature, the systematic errors in the reconstructed DOS associated with the temperature determination do not affect our main conclusions regarding the differences between the transient and the equilibrium spectra shown in Fig. 3(f).

Another source of systematic uncertainty in the reconstructed DOS is the possible error in the energy of the Fermi level after photoexcitation, arising from the difference between the plasma-induced renormalization of the Si valence band and that of the LHB. As shown in the main text (Sec. IV B), this difference is estimated to be ∼10 meV. Figure 10 compares the reconstructed DOS at $t = 0$ obtained using Fermi-level positions shifted by ±20 meV with respect to the value measured before the photoexcitation. These shifts correspond to twice the estimated uncertainty on E_F and provide a conservative estimate of the associated systematic error. Even in these cases, the reconstructed DOS supports our conclusions regarding the formation of in-gap states and differences between the transient and the equilibrium spectra shown in Fig. 3(f).

[1] Y. Murakami, D. Golež, M. Eckstein, and P. Werner, Photoinduced nonequilibrium states in Mott insulators, Rev. Mod. Phys. **97**, 035001 (2025), and references therein.

[2] C. N. Yang, η pairing and off-diagonal long-range order in a Hubbard model, Phys. Rev. Lett. **63**, 2144 (1989).

[3] T. Kaneko, T. Shirakawa, S. Sorella, and S. Yunoki, Photoinduced η-pairing in the Hubbard model, Phys. Rev. Lett. **122**, 077002 (2019).

[4] J. Li, D. Golež, P. Werner, and M. Eckstein, η-paired superconducting hidden phase in photodoped Mott insulators, Phys. Rev. B **102**, 165136 (2020).

[5] S. Ray and P. Werner, Photoinduced charge, spin, and orbital order in the two- orbital extended Hubbard model, Phys. Rev. B **110**, 214433 (2024).

[6] M. Eckstein, and P. Werner, Thermalization of a pump-excited Mott insulator, Phys. Rev. B **84**, 035122 (2011); Ultafast photo-carrier relaxation in Mott insulators with short-range spin correlation, Sci. Rep. **6**, 21235 (2016).

[7] J. H. Mentink and M. Eckstein, Ultrafast quenching of the exchange interaction in a Mott insulator, Phys. Rev. Lett. **113**, 057201 (2014).

[8] J. Li and M. Eckstein, Nonequilibrium steady-state theory of photodoped Mott insulators, Phys. Rev. B **103**, 045133 (2021).

[9] S. Ejima, F. Lange, and H. Fehske, Nonequilibrium dynamics in pumped Mott insulators, Phys. Rev. Res. **4**, L012012 (2022).

[10] S. Ray and P. Werner, Photo-induced ferromagnetic and superconducting orders in multi-orbital Hubbard models, Phys. Rev. B **110**, L041109 (2024).

[11] K. Kimura, H. Matsuzaki, S. Takaishi, M. Yamashita, and H. Okamoto, Ultrafast photoinduced transitions in charge density wave, Mott insulator, and metallic phases of an iodine-bridged platinum compound, Phys. Rev. B **79**, 075116 (2009); S. Iwai, M. Ono, A. Maeda, H. Matsuzaki, H. Kishida, H. Okamoto, and Y. Tokura, Ultrafast optical switching to a metallic state by photoinduced Mott transition in a halogen-bridged nickel-chain compound, Phys. Rev. Lett. **91**, 057401 (2003).

[12] H. Okamoto, T. Miyagoe, K. Kobayashi, H. Uemura, H. Nishioka, H. Matsuzaki, A. Sawa, and Y. Tokura, Photoinduced transition from Mott insulator to metal in the undoped cuprates Nd_2CuO_4 and La_2CuO_4, Phys. Rev. B **83**, 125102 (2011); H. Okamoto, H. Matsuzaki, T. Wakabayashi, Y. Takahashi, and T. Hasegawa, Photoinduced metallic state mediated by spin- charge separation in a one-dimensional organic Mott insulator, Phys. Rev. Lett. **98**, 037401 (2007).

[13] D. Fausti, R. I. Tobey, N. Dean, S. Kaiser, A. Dienst, M. C. Hoffmann, S. Pyon, T. Takayama, H. Takagi, and A. Cavalleri, Light-induced superconductivity in a stripe-ordered cuprate, Science **331**, 189 (2011).

[14] S. Kaiser, C. R. Hunt, D. Nicoletti, W. Hu, I. Gierz, H. Y. Liu, M. Le Tacon, T. Loew, D. Haug, B. Keimer, and A. Cavalleri, Optically induced coherent transport far above T_c in underdoped $YBa_2Cu_3O_{6-\delta}$, Phys. Rev. B **89**, 184516 (2014).

[15] K. Katsumi, M. Nishida, S. Kaiser, S. Miyasaka, S. Tajima, and R. Shimano, Near-infrared light-induced superconducting-like state in underdoped $YBa_2Cu_3O_y$ studied by c-axis terahertz third-harmonic generation, Phys. Rev. B **107**, 214506 (2023).

[16] T. Suzuki, T. Someya, T. Hashimoto, S. Michimae, M. Watanabe, M. Fujisawa, T. Kanai, N. Ishii, J. Itatani, S. Kasahara, Y. Matsuda, T. Shibauchi, K. Okazaki, and S. Shin, Photoinduced possible superconducting state with long-lived disproportionate band filling in FeSe, Commun. Phys. **2**, 115 (2019).

[17] M. Buzzi, D. Nicoletti, M. Fechner, N. Tancogne-Dejean, M. A. Sentef, A. Georges, T. Biesner, E. Uykur, M. Dressel, A. Henderson, T. Siegrist, J. A. Schlueter, K. Miyagawa, K. Kanoda, M.-S. Nam, A. Ardavan, J. Coulthard, J. Tindall, F. Schlawin, D. Jaksch, and A. Cavalleri, Photomolecular high- temperature superconductivity, Phys. Rev. X **10**, 031028 (2020).

[18] M. Mitrano, A. Cantaluppi, D. Nicoletti, S. Kaiser, A. Perucchi, S. Lupi, P. D. Pietro, D. Pontiroli, M. Riccò, S. R. Clark, D. Jaksch, and A. Cavalleri, Possible light-induced superconductivity in K_3C_{60} at high temperature, Nature (London) **530**, 461 (2016).

[19] M. Ligges, I. Avigo, D. Golež, H. U. R. Strand, Y. Beyazit, K. Hanff, F. Diekmann, L. Stojchevska, M. Kalläne, P. Zhou, K. Rossnagel, M. Eckstein, P. Werner, and U. Bovensiepen, Ultrafast doublon dynamics in photoexcited $1T$-TaS_2, Phys. Rev. Lett. **120**, 166401 (2018).

[20] L. Perfetti, P. A. Loukakos, M. Lisowski, U. Bovevensiepen, M. Wolf, H. Berger, S. Biermann, and A. Georges, Femtosecond dynamics of electronic states in the Mott insulator $1T$-TaS_2 by time resolved photoelectron spectroscopy, New J. Phys. **10**, 053019 (2008).

[21] L. Perfetti, P. A. Loukakos, M. Lisowski, U. Bovensiepen, H. Berger, S. Biermann, P. S. Cornaglia, A. Georges, and M. Wolf, Time evolution of the electronic structure of $1T$-TaS_2 through the insulator-metal transition, Phys. Rev. Lett. **97**, 067402 (2006).

[22] Z. Lenarčič and P. Prelovšek, Ultrafast charge recombination in photoexcited Mott-Hubbard insulators, Phys. Rev. Lett. **111**, 016401 (2013); Charge recombination in undoped cuprates, Phys. Rev. B **90**, 235136 (2014).

[23] S. M. Gilbertson, T. Durakiewicz, G. L. Dakovski, Y. Li, J.-X. Zhu, S. D. Conradson, S. A. Trugman, and G. Rodriguez, Ultrafast photoemission spectroscopy of the uranium dioxide Mott insulator: Evidence for a robust energy gap structure, Phys. Rev. Lett. **112**, 087402 (2014).

[24] D. Nevola, A. Bataller, A. Kumar, S. Sridhar, J. Frick, S. O'Donnell, H. Ade, P. A. Maggard, A. F. Kemper, K. Gundogdu, and D. B. Dougherty, Timescales of excited state relaxation in a-$RuCl_3$ observed by time-resolved two-photon photoemission spectroscopy, Phys. Rev. B **103**, 245105 (2021).

[25] G. Lantz, B. Mansart, D. Grieger, D. Boschetto, N. Nilforoushan, E. Papalazarou, N. Moisan, L. Perfetti, V. L. R. Jacques, D. Le Bolloc'h, C. Laulhé, S. Ravy, J-P Rueff, T. E. Glover, M. P. Hertlein, Z. Hussain, S. Song, M. Chollet, M. Fabrizio, and M. Marsi, Ultrafast evolution and transient phases of a prototype out-of-equilibrium Mott–Hubbard material, Nat. Commun. **8**, 13917 (2017).

[26] D. Wegkamp, M. Herzog, L. Xian, M. Gatti, P. Cudazzo, C. L. McGahan, R. E. Marvel, R. F. Haglund, Jr., A. Rubio, M. Wolf, and J. Stähler, Instantaneous bandgap collapse in photoexcited monoclinic VO_2 due to photocarrier doping, Phys. Rev. Lett. **113**, 216401 (2014).

[27] C. Sohrt, A. Stange, M. Bauer, and K. Rossnagel, How fast can a Peierls–Mott insulator be melted? Farad. Discuss. **171**, 243 (2014).

[28] C. Piovera, V. Brouet, E. Papalazarou, M. Caputo, M. Marsi, A. Taleb-Ibrahimi, B. J. Kim, and L. Perfetti, Time-resolved photoemission of Sr_2IrO_4, Phys. Rev. B **93**, 241114(R) (2016).

[29] O. Mehio, X. Li, H. Ning, Z. Lenarčič, Y. Han, M. Buchhold, Z. Porter, N. J. Laurita, S. D. Wilson, and D. Hsieh, A Hubbard exciton fluid in a photo-doped antiferromagnetic Mott insulator, Nat. Phys. **19**, 1876 (2023).

[30] Y. Kim and J. Lee, Time-resolved photoemission of infinitely periodic atomic arrangements: Correlation-dressed excited states of solids, npj Comput. Mater. **6**, 132 (2020).

[31] S. Modesti, L. Petaccia, G. Ceballos, I. Vobornik, G. Panaccione, G. Rossi, L. Ottaviano, R. Larciprete, S. Lizzit, and A. Goldoni, Insulating ground state of Sn/Si(111)-($\sqrt{3} \times \sqrt{3}$)R30°, Phys. Rev. Lett. **98**, 126401 (2007).

[32] G. Profeta and E. Tosatti, Triangular Mott-Hubbard insulator phases of Sn/Si(111) and Sn/Ge(111) surfaces, Phys. Rev. Lett. **98**, 086401 (2007).

[33] A. B. Odobescu, A. A. Maizlakh, N. I. Fedotov, and S. V. Zaitsev-Zotov, Electronic correlation effects and Coulomb gap in the Si(111)-($\sqrt{3} \times \sqrt{3}$)-Sn surface, Phys. Rev. B **95**, 195151 (2017).

[34] F. Ming, S. Johnston, D. Mulugeta, T. S. Smith, P. Vilmercati, G. Lee, T. A. Maier, P. C. Snijders, and H. H. Weitering, Realization of a hole-doped Mott insulator on a triangular silicon lattice, Phys. Rev. Lett. **119**, 266802 (2017).

[35] M. Iannetti, S. Modesti, G. Di Santo, M. Caputo, P. M. Sheverdyaeva, P. Moras, F. Chiapolino, T. Cea, C. Tresca, E. Tosatti, and G. Profeta, The electronic structure of a doped Mott-Hubbard surface, Phys. Rev. B **112**, 075159 (2025).

[36] F. Ming, X. Wu, C. Chen, K. D. Wang, P. Mai, T. A. Maier, J. Strockoz, J. W. F. Venderbos, C. González, J. Ortega, S. Johnston, and H. H. Weitering, Evidence for chiral superconductivity on a silicon surface, Nat. Phys. **19**, 500 (2023).

[37] Y.-L. Xiong, J.-Q. Guan, R.-F. Wang, C.-L. Song, X.-C. Ma, and Q.-K. Xue, Experimental observation of pseudogap in a modulation- doped Mott insulator: Sn/Si(111)-($\sqrt{3} \times \sqrt{3}$)R30°, Chinese Phys. B **31**, 067401(2022).

[38] P. Hansmann, T. Ayral, L. Vaugier, P. Werner, and S. Biermann, Long-range Coulomb interactions in surface systems: A first principles description within self-consistently combined *GW* and dynamical mean field theory, Phys. Rev. Lett. **110**, 166401 (2013).

[39] M. Zahedifar and P. Kratzer, Phonon-induced electronic relaxation in a strongly correlated system: The Sn/Si(111) ($\sqrt{3} \times \sqrt{3}$) adlayer revisited, Phys. Rev. B **100**, 125427 (2019).

[40] NFFA-Europe, Time-Resolved PES and Spin Polarization (SPRINT), https://www.trieste.nffa.eu/techniques/spectroscopy/time-resolved-pes-and-spin-polarization-sprint/.

[41] R. Cucini,T. Pincelli, G. Panaccione, D. Kopic, F. Frassetto, P. Miotti, G. M. Pierantozzi, S. Peli, A. Fondacaro, A. De Luisa, A. De Vita, P. Carrara, D. Krizmancic, D. T. Payne, F. Salvador, A. Sterzi, L. Poletto, F. Parmigiani, G. Rossi, and F. Cilento, Coherent narrowband light source for ultrafast photoelectron spectroscopy in the 17–31 eV photon energy range, Struct. Dyn. **7**, 014313 (2020).

[42] R. I. G. Uhrberg, H. M. Zhang, T. Balasubramanian, S. T. Jemander, N. Lin, and G. V. Hansson, Electronic structure of Sn/Si (111) $\sqrt{3} \times \sqrt{3}$: Indications of a low-temperature phase, Phys. Rev. B **62**, 8082 (2000); J. Lobo, A. Tejeda, A. Mugarza, and E. G. Michel, Electronic structure of Sn/Si(111)-($\sqrt{3} \times \sqrt{3}$) *R*30° as a function of Sn coverage, *ibid.* **68**, 235332 (2003).

[43] M. Alonso, R. Cimino, and K. Horn, Surface photovoltage effects in photoemission from metal-GaP (110) interfaces: Importance for band bending evaluation, Phys. Rev. Lett. **64**, 1947 (1990).

[44] H. Dember, Photoelectromotive force in cuprous oxide crystals, Phys. Z. **32**, 554 (1931).

[45] Shin-ichiro Tanaka, Utility and constraint on the use of pump-probe photoelectron spectroscopy for detecting time-resolved surface photovoltage, J. Electron Spectrosc. Relat. Phenom. **185**, 152 (2012).

[46] T. Zhang, Z.-C. Huang-Fu, Y. Qian, H. Gao, J. B. Brown, and Y. Rao, Photoinduced surface electric fields and surface population dynamics of GaP(100) photoelectrodes, J. Phys. Chem. C **126**, 6531 (2022).

[47] S. L. Yang, J. A Sobota, P. S. Kirchmann, and Z. X Shen, Electron propagation from a photo-excited surface: Implications for time-resolved photoemission, Appl. Phys. A **116**, 85 (2014).

[48] P. Siffalovic, M. Drescher, and U. Heinzmann, Femtosecond time-resolved core-level photoelectron spectroscopy tracking surface photovoltage transients on *p*–GaAs, Europhys. Lett. **60**, 924 (2002).

[49] P. Vashishta and R. K. Kalia, Universal behavior of exchange-correlation energy in electron-hole liquid, Phys. Rev. B **25**, 6492 (1982).

[50] J. Kanasaki, H. Tanimura, K. Tanimura, P. Ries, W. Heckel, K. Biedermann, and T. Fauster, Ultrafast dynamics in photoecited valence-band states of Si studied by time- and angle-resolved photoemission spectroscopy of bulk direct transitions, Phys. Rev. B **97**, 035201 (2018).

[51] P. L. Gourley and J. P. Wolfe, Properties of the electron-hole liquid in Si: Zero stress to the high-stress limit, Phys. Rev. B **24**, 5970 (1981); J. Bokor and N. J. Halas, Time-resolved study of silicon surface recombination, IEEE J. Quantum Electron. **25**, 2550 (1989).

[52] The spectrum measured 1 ps before the pump pulse in the equilibrium MI phase has a residual intensity at the Fermi level because of the experimental resolution and the 60 meV energy broadening caused by the inhomogeneity of the SPV induced by the pump.

[53] F. Giustino, Electron-phonon interactions from first principles, Rev. Mod. Phys. **89**, 015003 (2017).

[54] F. Petocchi, C. W. Nicholson, B. Salzmann, D. Pasquier, O. V. Yazyev, C. Monney, and P. Werner, Mott versus hybridization gap in the low- temperature phase of 1*T*-TaS_2, Phys. Rev. Lett. **129**, 016402 (2022), and references therein.

[55] D. R. Baykusheva, H. Jang, A. A. Husain, S. Lee, S. F. R. TenHuisen, P. Zhou, S. Park, H. Kim, J.-K. Kim, H-D. Kim, M. Kim, S.-Y. Park, P. Abbamonte, B. J. Kim, G. D. Gu, Y. Wang, and M. Mitrano, Ultrafast renormalization of the on-site Coulomb repulsion in a cuprate superconductor, Phys. Rev. X **12**, 011013 (2022).

[56] T. Lojewski *et al.*, Photoinduced charge transfer renormalization in NiO, Phys. Rev. B **110**, 245120 (2024).

[57] Indeed, the low optical absorption coefficient of Si at 800 nm $-10^3\,\mathrm{cm}^{-1}$- limits the maximum heating of the Si substrate after a pump pulse at about 1 K. The surface layer absorbs less than 0.1% of the photons because the maximum excitation density estimated from the spectra of Fig. 2(a) is 0.02 per cell and the pump pulse gives 30 photons per surface unit cell. Assuming a surface specific heat comparable to that of bulk Si, this corresponds to a maximum increase in the the surface-lattice temperature of the order of 1 K. If carrier multiplication by impact scattering occurs after photoexcitation, the number of photons initially absorbed by the surface layer would be even smaller than estimated above, implying an even smaller lattice temperature increase.

[58] S. S. Bakshi and P. Majumdar, Distinct charge and spin recovery dynamics in a photo-excited Mott insulator, Phys. Rev. Lett. **133**, 256501 (2024).

[59] www.trieste.nffa.eu.

[60] S. Modesti, Data for "Transient photoexcited state of a small-gap quasi-two-dimensional Mott-Hubbard insulator" [Dataset], Zenodo, 2026, https://zenodo.org/records/18510537.